Mutations in the Drosophila rough deal gene affecting RZZ kinetochore function

Alexandra Menant, Roger Karess

Biol. Cell (2020) **112,** 1–16 DOI: 10.1111/boc.201900105

Research article

Mutations in the *Drosophila rough deal* gene affecting RZZ kinetochore function

Alexandra Menant[2] and Roger E. Karess[1]

Université de Paris, CNRS, Institut Jacques Monod, 15 rue Hélène Brion, Paris 75013, France

Background. The RZZ complex, composed of the proteins Rough-Deal (Rod), Zw10 and Zwilch, plays a central role in the spindle assembly checkpoint (SAC), which assures proper sister chromatid segregation during mitosis. RZZ contributes to the regulation of the spindle assembly checkpoint by helping to recruit Mad1–Mad2 and the microtubule motor dynein to unattached kinetochores. It is an important component of the outer kinetochore and specifically the fibrous corona whose expansion is believed to facilitate microtubule capture. How RZZ carries out its diverse activities is only poorly understood. The C-terminal region of the Rod subunit is relatively well-conserved across metazoan phylogeny, but no function has been attributed to it.

Results. To explore the importance of the Rod_C domain in RZZ function in *Drosophila*, we generated a series of point mutations in a stretch of 200 residues within this domain and we report here their phenotypes. Several of the mutations profoundly disrupt recruitment of RZZ to kinetochores, including one in a temperature-sensitive manner, while still retaining the capacity to assemble into a complex with Zw10 and Zwilch. Others affect aspects of dynein activity or recruitment at the kinetochore.

Conclusions and Significance. These results suggest that the Rod_C domain participates in the protein interactions necessary for RZZ recruitment and functionality at kinetochores.

Additional supporting information may be found online in the Supporting Information section at the end of the article.

Introduction

The spindle assembly checkpoint (SAC) assures proper sister chromatid segregation during mitosis [Musacchio, 2015]. The SAC surveys the attachment state of kinetochores and inhibits anaphase onset until all kinetochores are stably attached to the spindle. The central checkpoint components Mad1 and Mad2 are recruited onto unattached kinetochores at the start of mitosis, where together they catalyse the formation of an 'anaphase inhibitor' of the E3 ubiquitin ligase called the anaphase promoting complex, thus blocking anaphase onset. Once a kinetochore has properly attached to spindle fibres, Mad1–Mad2 is depleted from the kinetochore and transport along the microtubules in a dynein-dependent process called variously shedding, streaming or stripping. This mechanism is believed to be one of the major pathways by which the checkpoint activity is turned off.

The RZZ complex, composed of the proteins Rough-Deal (Rod), Zw10 and Zwilch, plays a central role in the SAC [Karess, 2005]. It is an important

[1]To whom correspondence should be addressed (email: roger.karess@ijm.fr)
[2]Current address: Institute for Integrative Biology of the Cell (I2BC), Université Paris-Saclay, CEA, CNRS, 91198 Gif-sur-Yvette, France
Key words: Dynein, Kinetochore, RZZ, Spindle Assembly Checkpoint.
Abbreviations: BN-PAGE, Blue Native Polyacrylamide Gel Electrophoresis; DLIC, Dynein Light Intermediate Chain; GFP, Green Fluorescent Protein; kDa, kilodaltons; K-MT, kinetochore-microtubule; RFP, Red Fluorescent Protein; Rod, Rough-Deal; RZZ, Rough-Deal (Rod), Zw10 and Zwilch; SAC, Spindle Assembly Checkpoint; SDS, Sodium Dodecyl Sulfate

component of the outer kinetochore and specifically the fibrous corona [Basto et al., 2004; Sacristan et al., 2018], whose expansion is believed to facilitate microtubule capture. RZZ contributes to the regulation of the SAC by helping to recruit Mad1–Mad2 and dynein along with its associated regulatory proteins to unattached kinetochores [Buffin et al., 2005; Chan et al., 2009; Gama et al., 2017; Griffis et al., 2007; Kops et al., 2005; Starr et al., 1998].Thus RZZ is involved not only in activating the checkpoint (by recruiting Mad1–Mad2) but also in inactivating it, via dynein-dependent streaming of RZZ and Mad1–Mad2. RZZ and its cofactor Spindly are also implicated in regulating kinetochore-microtubule (K-MT) attachments [Cheerambathur et al., 2013; Gassmann et al., 2008, 2010].

RZZ has an apparent molecular weight of about 700–800 kDa and contains two copies of each of the three subunits, Rod, Zw10 and Zwilch, with the 240-kDa Rod subunit serving as the scaffold [Civril et al., 2010; Mosalaganti et al., 2017; Scaerou et al., 2001; Williams et al., 2003]. Secondary structure predictions of Rod [Civril et al., 2010] reveal an N-terminal region folding into a β propeller and a long α-solenoid region extending to the C-terminus. A model based on structural analysis and low-resolution cryo-EM of recombinant mammalian RZZ [Mosalaganti et al., 2017] shows an elongated axially symmetrical protein with the two Rod subunits assembling in a head-to-tail manner that juxtaposes the β propeller of one subunit with the C-terminal domain of the other (Figures 1A and 2A). A Zwilch subunit associates with each head-tail domain, and the two Zw10 subunits are symmetrically bound in the middle, in association with a domain of Rod with homology to Sec39.

How RZZ carries out its diverse activities is only poorly understood. Even the pathways leading to its recruitment and accumulation at unattached kinetochores are not yet clear. Recent reports suggest that interactions with Bub1 and Knl1/Zwint complex [Caldas et al., 2015; Silio et al., 2015; Zhang et al., 2015] contribute but are not sufficient for RZZ recruitment at kinetochores. Regarding the domains of RZZ involved in its kinetochore recruitment, Gama et al. [2017] found that a sub-complex containing only tagged Rod and Zw10 is recruitment-competent in *C. elegans*. In human cells a Rod construct lacking the N-terminal β-propeller fold can still bind Zw10 (though not Zwilch) and still target kinetochores, though it could no longer generate expanded kinetochores [Gama et al., 2017].

The Rod_C domain (pfam10493) that covers approximately 550 residues towards the end of the Rod α-solenoid, is common to all metazoan members of the Rod family [Marchler-Bauer et al., 2017]. It is notably absent from the structurally related, but functionally distinct, Nag proteins, implicated in Golgi trafficking [Civril et al., 2010]. However it displays no obvious structural similarity to other conserved protein domains, and no specific function has been attributed to it. We previously described the phenotype of a *Drosophila* mutant called rod^{fZ3} [Defachelles et al., 2015a], caused by a single amino acid change in the Rod_C domain. This mutation greatly reduces the recruitment of RZZ and Mad1–Mad2 to kinetochores, and in addition has a semi-dominant effect on dynein-mediated streaming of RZZ during metaphase (Defachelles et al., 2015a).

To further explore the contribution of the Rod_C domain in RZZ function in *Drosophila*, we generated a series of additional point mutations within this domain. Some of these interfere with RZZ kinetochore recruitment and others affect dynein activity, while maintaining the RZZ complex. Thus the Rod_C domain appears to have an important function in RZZ activity.

Results

Interdependencies of the three RZZ components for assembly and kinetochore recruitment in *Drosophila*

Each of the three RZZ components had been previously shown to be necessary for kinetochore localisation of the two others, based largely on immunostaining of fixed material [Scaerou et al., 2001; Williams and Goldberg, 1994; Williams et al., 1992; Williams et al., 2003]. To complete these studies, we (i) assayed fluorescently tagged RZZ recruitment to kinetochores during mitosis in live neuroblasts; (ii) employed co-immunoprecipitation of RZZ from larval brain extracts; and (iii) assayed the integrity of the RZZ complex by Blue Native polyacrylamide gel electrophoresis (BN-PAGE) [Fiala et al., 2011; Swamy et al., 2006].

We had previously reported that in wild-type *Drosophila* neuroblasts expressing both GFP-Zw10

Figure 1 | **See Legend on next page**

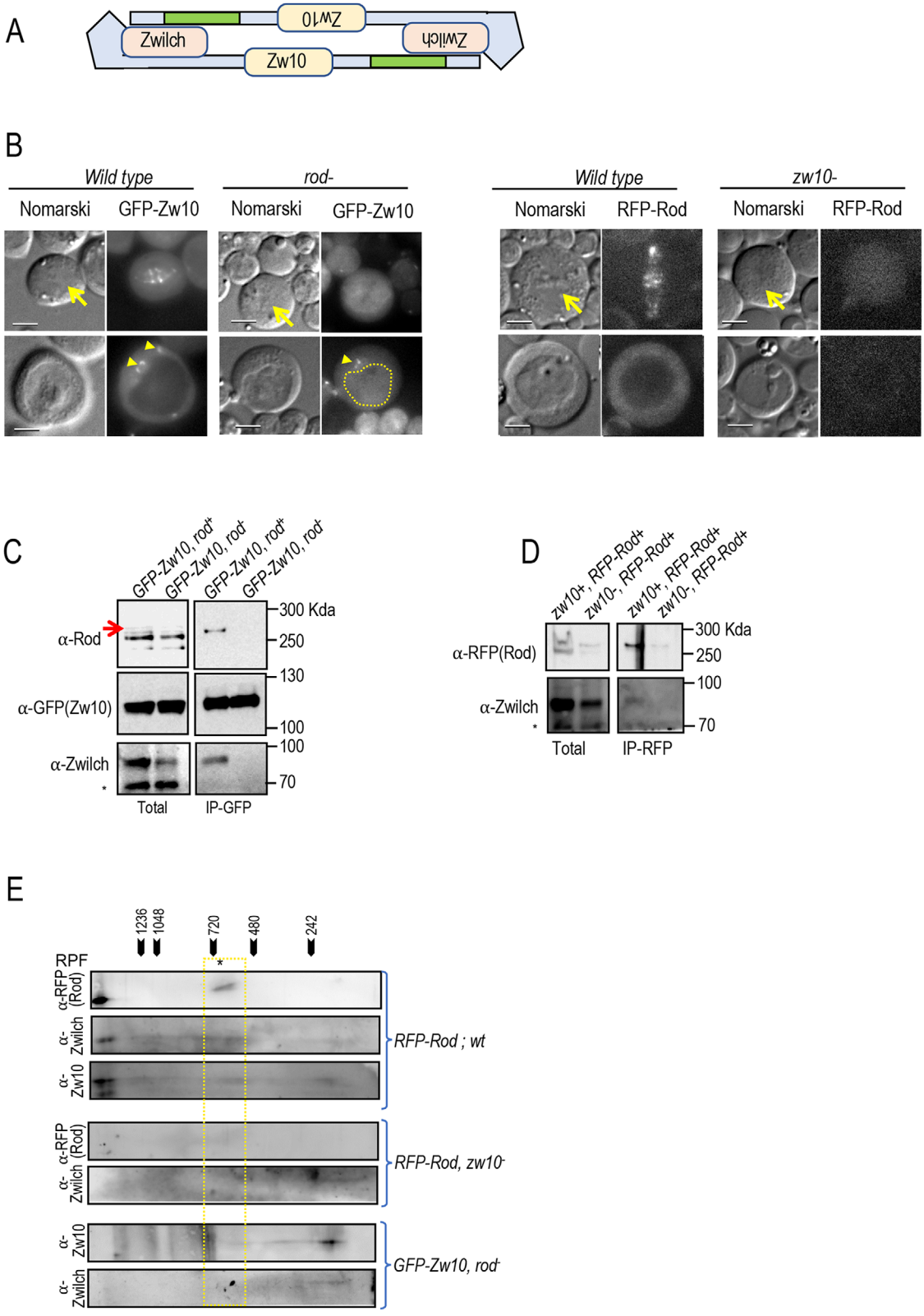

Figure 1 | Rod and Zw10 are both required for kinetochore recruitment and for the integrity of a high molecular weight complex containing Zwilch

(**A**) A model of RZZ based on the study of (Mosalaganti et al., 2017). The Rod subunits are blue, with the Rod_C domain marked in green. (**B**) In wild-type larval neuroblasts, GFP-Zw10 and RFP-Rod are recruited to kinetochores and spindle during mitosis (top panels) and are cytoplasmic during interphase (bottom panels). Zw10 but not Rod is enriched in Golgi elements (arrowheads, bottom panels), as has been described [Defachelles et al., 2015b]. In *rod*$^{-}$ null mutant cells (second from left), GFP-Zw10 is no longer on the mitotic apparatus but is still present during interphase in the cytoplasm and in Golgi. It is also no longer excluded from the interphase nucleus. In *zw10* mutant cells (far right), RFP-Rod is barely detectable in the cytoplasm of interphase cells and shows no enrichment on kinetochores during mitosis. Live images of third instar larval brain cells of the indicated genotypes. Arrows indicate position of metaphase plates. Scale bar 5 microns. (**C**) Rod is required for the co-immunoprecipitation of GFP-Zw10 with Zwilch. Protein extracts (left) of wild-type or *rod* null mutant third instar larval brains expressing GFP-Zw10 were immunoprecipitated with anti-GFP (right) and assayed by Western blot for the presence of co-immunoprecipitating proteins. In the *rod* mutant extracts, GFP-Zw10 no longer coprecipitated with Zwilch. Note that the anti-Rod antibody is impure, and Rod is only a minor band (arrow) in the total extract. This band is, however, clearly detected in the immunoprecipitates wild-type (*rod*$^{+}$) but not *rod*$^{-}$. Star (*) denotes non-specific protein detected by anti-Zwilch. (**D**) Zw10 is required for the stability of RFP-Rod. Western blot analysis of protein extracts (left) and anti-RFP immunoprecipitates (right) of wild-type or *zw10* null mutant larval brains expressing RFP-Rod. In whole extracts of *zw10* mutant cells, RFP-Rod is significantly reduced; Zwilch somewhat less so. In immunoprecipitates, the amount of co-precipitating Zwilch is below detection levels. Star (*) denotes nonspecific protein detected by anti-Zwilch. (**E**) Analysis of the RZZ complex by BN-PAGE. Third instar larval brain protein extracts were first resolved by native electrophoresis and then further resolved by SDS-PAGE in the second dimension to separate individual components. Genotypes of brains are indicated on the right. Immunoblotting was performed with anti-RFP (for Rod), anti- Zw10 and anti-Zwilch antibodies (as indicated on the left). Molecular weight markers (above the blot) indicate approximate size of the migrating native complexes. In the extracts expressing RFP-Rod in a wild-type background, a band enriched at approximately 700 kDa (indicated by a star), contains RFP-Rod, Zw10 and Zwilch (yellow rectangle). In *rod*$^{-}$ extracts expressing GFP-Zw10, there is no major band at 700 kDa. Instead, both Zw10 and Zwilch are found in lower molecular weight species. In extracts of *zw10*$^{-}$RFP-Rod individuals, Rod and Zwilch are undetectable around 700 kDa.

and RFP-Rod, the two proteins were simultaneously recruited to and shed from kinetochores [Defachelles et al., 2015b], suggesting that they had indeed assembled into a functional RZZ complex. During interphase, both GFP-Zw10 and RFP-Rod were diffusely cytoplasmic but only GFP-Zw10 labelled cytoplasmic Golgi elements ([Defachelles et al., 2015b], confirmed in Figure 1B, lower panels).

In neuroblasts from *rod*$^{-}$ null mutant larvae, GFP-Zw10 remained detectable during the interphase in Golgi elements, while, as expected [Scaerou et al., 2001], it did not accumulate on the spindle during mitosis (Figure 1B, *left*).These results suggest that the Golgi localisation of Zw10 does not depend on an intact RZZ. In addition, GFP-Zw10 was no longer excluded from the interphase nucleus in *rod*$^{-}$ cells, but appeared freely diffusible throughout the cell. In *zw10*$^{-}$ mutant cells, the levels of RFP-Rod were greatly reduced relative to wild type (Figure 1B, *right*). Little or no RFP-Rod fluorescence was detectable at kinetochores or cytoplasm in either mitotic or interphase cells, suggesting that Rod is unstable in the absence of Zw10 (see below).

We next asked if Rod was required for the formation of a stable complex containing Zwilch and Zw10. We found that whereas immunoprecipitating GFP-Zw10 from wild-type extracts co-precipitated Zwilch robustly, Zwilch was completely absent from anti-GFP-Zw10 precipitates of *rod*$^{-}$mutant extracts (Figure 1C, *right*). This result is consistent with the model that Rod serves as a scaffold binding the two other subunits. In the absence of Rod, Zwilch (but not GFP-Zw10) seemed to be slightly destabilised in whole extracts (Figure 1C, *left*). Blots of whole extracts from *zw10* mutant cells (Figure 1D, *left*) confirmed that RFP-Rod was significantly reduced in the absence of Zw10, consistent with the fluorescence results above. Because the level of RFP-Rod is so low in *zw10* mutant cell extracts, we could not determine by co-immunoprecipitation whether Rod-Zwilch interactions occur in the absence of Zw10 (Figure 1D, *right*).

Figure 2 | Mutations in the Rod_C domain examined in this study

(**A**) The model of RZZ based on the study of Mosalaganti et al. [2017] and the different domains of the Rod protein [Civril et al., 2010; Marchler-Bauer et al., 2017]. (**B**) Clustal-W alignment of the C-terminal half of the Rod_C domains from four vertebrates (human, mouse, chicken, zebrafish) and four dipterans (*Aedes aegypti*, *Drosophila grimshawi*, *Drosophila willistoni*, *Drosophila melanogaster*). Regions of predicted alpha helix across the alignment are indicated by green bars. The new *D. melanogaster* Rod mutations described here (numbered 1–17) corresponding to one or two altered residues are delimited by the red boxes, and the corresponding substitutions are indicated below in blue. The dotted box corresponds to the *rod*^{Z3} mutation [Defachelles et al., 2015a] (see also Table 1).

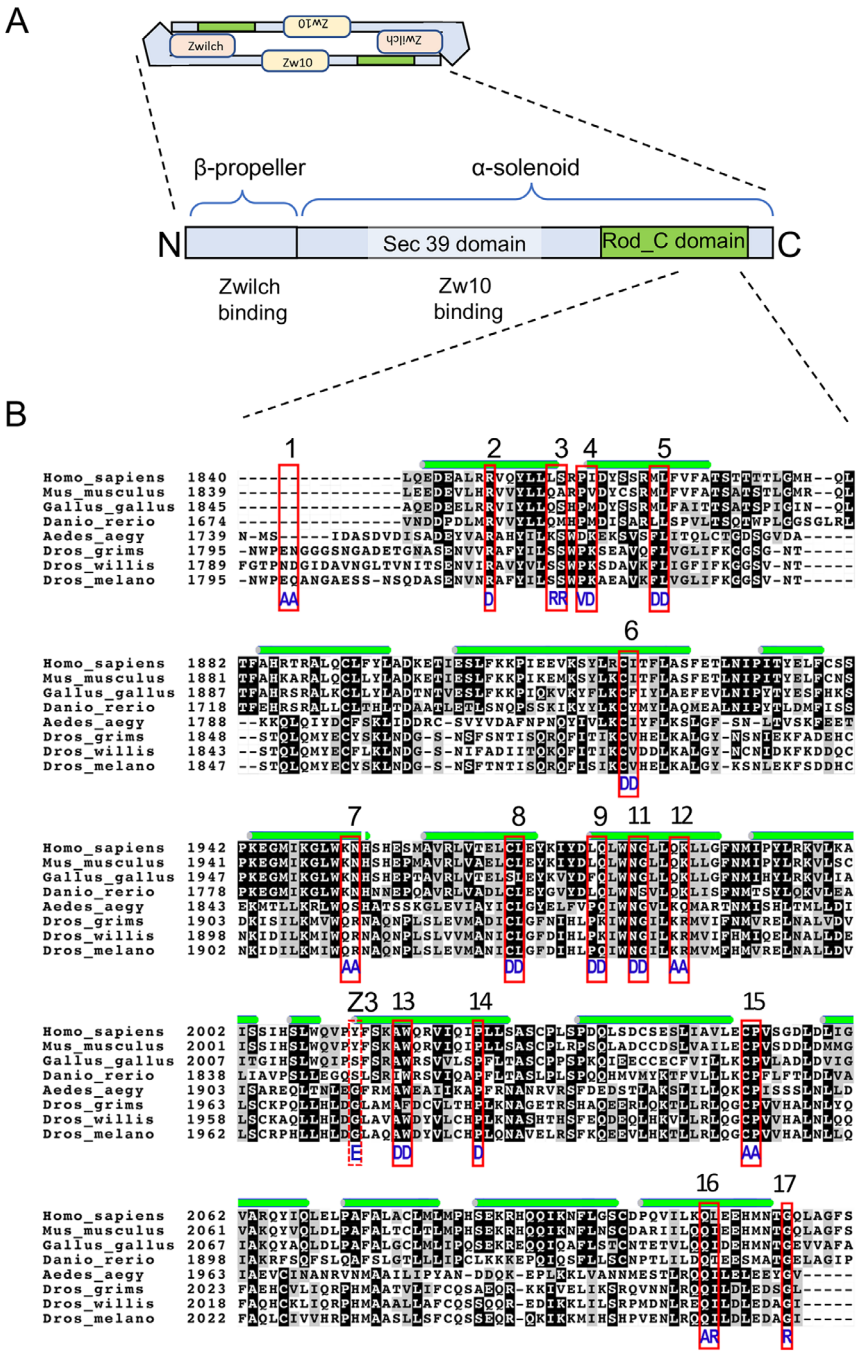

The native RZZ complex (represented schematically in Figure 1A) has an apparent molecular mass of about 700–800 kDa [Mosalaganti et al., 2017; Williams et al., 2003] consistent with an assembly corresponding to two copies each of Rod, Zw10 and Zwilch [Mosalaganti et al., 2017; Williams et al., 2003]. By employing BN-PAGE, a technique capable of detecting and analysing high molecular weight multi-subunit complexes [Fiala et al., 2011; Swamy et al., 2006], we found that RFP-Rod, Zw10 and Zwilch were indeed enriched in a band migrating approximately at 700 kDa (Figure 1E, top lanes), in extracts of RFP-Rod expressing brains. In extracts of GFP-Zw10-expressing *rod*$^{-}$ brains however, the majority of the GFP-Zw10 and Zwilch signals were displaced towards lower molecular weights (Figure 1E, bottom lanes). (A weak Zw10 signal persisting around 400–700 kDa suggests that Zw10 may also be part of large complexes other than RZZ, perhaps related to its function in vesicle trafficking.) In the *zw10*$^{-}$ extracts (Figure 1E middle lanes), RFP-Rod is undetectable by BN-PAGE. Recently, it was shown *in vitro* that mammalian Rod is unstable in the absence of Zw10 and Zwilch [Mosalaganti et al., 2017] and it was reported in C. *elegans* that Rod is also destabilised in the absence of Zwilch [Gama et al., 2017]. All these data suggest that the assembly of the entire complex is required for Rod stability and to a lesser extent for Zwilch stability but not for Zw10.

Taken together with other published studies, these results confirm that the recruitment of Rod, Zw10 and Zwilch to kinetochores is mutually interdependent in *Drosophila* and suggests further that the RZZ complex is already preassembled in the cytoplasm, presumably during interphase and that this assembly is a pre-requisite for its recruitment to kinetochores. It also implies that, if RFP-Rod signal is detectable in the cytoplasm, it is most likely in a stable complex with Zw10 and Zwilch.

New mutations in the Rod_C domain

To further explore the contribution of the Rod_C domain to the RZZ function, we generated a series of 16 additional point mutations (named M1–M17; there is no M10) in a stretch of 200 residues covering the second half of this region, in proximity to the lesion of previously described *rod*^{Z3} (Figure 2, Table 1). In most cases, we selected residues or residue pairs that had been conservatively substituted or remained identical either within diptera or across metazoans (Figure 2B) and replaced them by residues with different properties, such as acidic for basic, or charged for hydrophobic (summarized in Table 1). The majority of the most highly conserved residues in the Rod_C domain reside within the predicted short α-helical stretches comprising the α-solenoid.

These mutations were introduced in a previously validated RFP-Rod transgenic construct expressed from its natural promoter that fully rescued a *rod* null mutant [Buffin et al., 2005].

Hereafter, the mutant alleles carried by these transgenes are referred to as *RFP-rod*^{M1}, *RFP-rod*^{M2} etc. and the corresponding proteins are RFP-Rod^{M1} etc. Transgenic fly stocks bearing these *RFP-rod* mutations were established and examined by genetics, biochemistry and cell biology. Each line was characterised for its ability to complement a homozygous null *rod* mutant, and for the ability of the RFP-Rod^{M} variant protein to accumulate on kinetochores, both in the presence of an endogenous wild-type copy of Rod, and in homozygous *rod*$^{-}$ null cells.

Of the 16 *RFP-rod* transgenic alleles examined (Table 1), four (*M8, M12, M13* and *M16*) produced too little stable mutant RFP-Rod^{M} protein, even in a *rod*$^{+}$ background, to conclude anything about their functionality. They were therefore excluded from further study. Of the remaining mutant lines, *RFP-rod*^{M5} and *RFP-rod*^{M6} failed to rescue the lethality of *rod*$^{-}$ null mutant animals; *RFP-rod*^{M11} showed only weak complementation, allowing *rod*$^{-}$ flies to eclose, but generally not to survive, and failed to repair the characteristic rough eye phenotype. Three alleles (mutants *M4, M7, M9*) restored viability, but the resulting flies were sterile: the females laying eggs that failed to develop (maternal effect lethal), even when the zygotes were genetically *rod*$^{+}$. *RFP-rod*^{M15} proved to be temperature sensitive: lethal when raised at 29°C but viable and fertile when raised at 18°C (see below). The remaining five transgenic alleles (*RFP-rod*^{M} mutants *M1, M2, M3, M14, M17*) were able to fully complement the null *rod* homozygote, producing viable fertile adults of normal appearance. Overall, these results indicate that mutations in this part of the protein domain can impact RZZ function and are consistent with an important role for the Rod_C domain.

Table 1 | Summary of the examined mutations and their phenotypes

Mutant Transgene			rescue of *rod* null lethality	recruitment to kinetochore in *rod*$^-$	RZZ streaming	
Number	Site	Lesion			*rod*$^+$	*rod*$^-$
M1	E1798, Q1799	AA	+	+	+	+
M2	R1817	D	+	+	+	+
M3	S1823, S1824	RR	+	+	+	+
M4	P1826, K1827	VD	+ MEL/st	+	+	+
M5	F1833, L1834	DD	–	greatly reduced (Q)	+	–
M6	C1880, V1881	DD	–	greatly reduced (Q)	+	–
M7	Q1912, R1973	AA	+ MEL/st	+	+(Q)	– (Q)
M8*	C1928, L1929	DD	–*	low	ND	ND
M9	P1936, Q1937	DD	+ MEL/st	+	low (Q)	– (Q)
M11	N1940, G1941	DD	+/–	low (Q)	low (Q)	– (Q)
M12*	K1944, R1945	AA	– *	low	ND	ND
M13*	A1977, W1978	DD	– *	low	ND	ND
M14	P1985	D	+	+	+	+
M15	C2011, P2012	AA	+ (18°) – (29°)	greatly reduced (29°)(Q)	+ (29°)	low (25°)
M16*	Q2066, I2067	AR	– *	low	ND	ND
M17	G2074	R	+	+	+	ND

MEL: Maternal Effect Lethal
st : sterile
* These mutant variants were poorly expressed or unstable even in *rod*$^+$ background.
+ (for kinetochore recruitment): qualitatively normal.
low: qualitatively low
Q: Quantitated in Figs 3, 4 and/or 5
ND: not determined

Some mutations in the Rod_C domain profoundly inhibit RZZ recruitment to kinetochores without affecting RZZ complex assembly

While all 12 RFP-Rod^M mutant proteins examined were recruited to kinetochores in a *rod*$^+$ context, four of them (mutants M5, M6, M11 and M15) displayed reduced kinetochore localisation in *rod*$^-$ neuroblasts (Table 1), consistent with their reduced ability to rescue *rod*$^-$ homozygotes. *RFP-rod*^{M} alleles *M5, M6* and *M11* all replaced pairs of highly conserved uncharged residues within predicted α-helices with negatively charged aspartates (Figure 2B, Table 1). In a *rod*$^-$ background, the kinetochore recruitment of these proteins was very low in the majority of cells of both RFP-Rod^{M5} and RFP-Rod^{M6} but somewhat higher in the case of RFP-Rod^{M11} (Figure 3A, *left*). This was confirmed by quantification of the RFP signal normalised to the signal from outer kinetochore component Spc25-GFP (Figure 3B). A brief (15 min) colchicine treatment releases the kinetochores from K-MTs and leads to a significant increase in kinetochore recruitment of M5, M6 and M11 in the wild-type (*rod*$^+$) context (Figure 3A *right*, Figure 3B); however, in *rod*$^-$ cells kinetochore signals of these three RFP-Rod^M variants remained essentially unchanged.

We next asked if RFP-Rod^{M5} and RFP-Rod^{M6} were competent for assembly into a complex with Zw10 and Zwilch. The levels of RFP-Rod^{M5} were similar in *rod*$^+$ and *rod*$^-$ brain extracts, showing that the stability of the mutant protein is not affected (Figure 3C). Similar results were found for RFP-Rod^{M6} (data not shown). This is consistent with the strong cytoplasmic RFP signal visible in interphase *RFP-Rod*^{M5} and *RFP-Rod*^{M6}; *rod*$^-$ cells. Anti-RFP immunoprecipitates of RFP-Rod^{M5} co-immunoprecipitated Zwilch and Zw10 equally well from *rod*$^+$ and *rod*$^-$ tissue extracts, suggesting that the assembly of the RZZ complex is not affected (Figure 3C). BN-PAGE analysis confirmed that RFP-Rod^{M5}, Zw10 and Zwilch co-migrated as part of a ~700-kDa complex in both *rod*$^+$ and *rod*$^-$ extracts (Figure 3D). Together these results indicate that both RFP-Rod^{M5} and RFP-Rod^{M6} profoundly interfere with the recruitment of RZZ to kinetochores but do not disrupt RZZ complex assembly.

Figure 3 | See Legend on next page

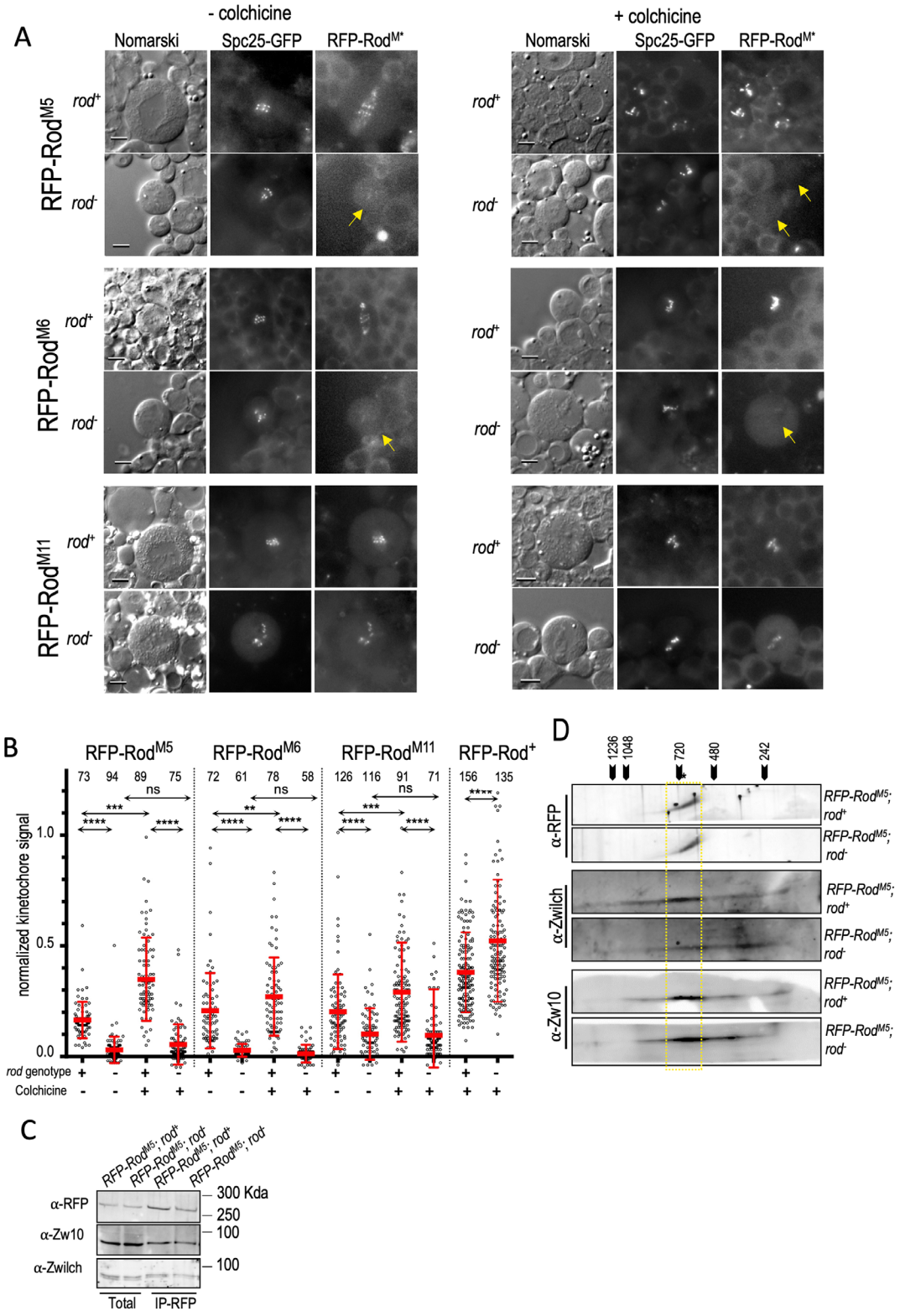

Figure 3 | RFP-Rod^{M5} and RFP-Rod^{M6} disrupt RZZ recruitment to kinetochores but not RZZ assembly
(**A**) Kinetochore recruitment of RFP-Rod^{M5} and RFP-Rod^{M6} is greatly reduced in a *rod*$^{-}$ background, and RFP-Rod^{M11} is moderately reduced. Live imaging of untreated (left) or colchicine-treated (right) larval brain cells expressing the indicated *RFP-Rod*^{M} transgenesin *rod*$^{+}$or *rod*$^{-}$ background. Spc25-GFP, a stable component of the KMN complex, marks the kinetochores. Yellow arrows indicate chromosomes with little or no RFP-Rod^{M} signal. Note the cytoplasmic signal in interphase *rod*$^{-}$ cells, indicating the presence of stable RFP-Rod^{M}, despite its inability to accumulate on kinetochores. Scale bar 5 microns. (**B**) Quantitation of RFP-Rod^{M5}, RFP-Rod^{M6} and RFP-Rod^{M11} kinetochore signals in *rod*$^{+}$ and *rod*$^{-}$ cells, normalised to that of Spc25-GFP, either untreated or treated with colchicine for 15 min. Each dot is the measurement of a single mitotic cell. Red lines correspond to the mean and SD for each set. In the *rod*$^{+}$ background, the brief colchicine treatment significantly raises the average localised RFP signal (****, $p < 0.006$, Mann–Whitney test), for all three mutant proteins, whereas in the *rod*$^{-}$ there is no significant change (ns). RFP-Rod^{M5} and RFP-Rod^{M6} show little if any kinetochore recruitment in the absence of endogenous wild-type Rod. RFP-Rod^{M11} kinetochore levels are reduced in *rod*$^{-}$ cells, but remain well above the average levels for Rod^{M5} and Rod^{M6}. For comparison, quantitation of kinetochore signals of wild-type RFP-Rod^{+}, in *rod*$^{+}$ and *rod*$^{-}$ cells treated with colchicine is also shown. (Note that this is the 18°C data set also used in Figure 4D). Number of cells analysed per condition is indicated. (**C**) RFP-Rod^{M5} co-immunoprecipitates with Zw10 and Zwilch equally well from *rod*$^{+}$ and *rod*$^{-}$ tissue extracts. Western blot of total protein extracts (left) and anti-RFP immunoprecipitates (right), from the third instar larval brains, revealed with anti-RFP, anti-Zw10 and anti-Zwilch antibodies. (**D**) RFP-Rod^{M5} can assemble into a high molecular weight RZZ complex in the presence or absence of wild-type Rod. The R^{M5}ZZ complex was analysed by BN-PAGE, migrating as a native complex in the first (horizontal) dimension, then as separate subunits in the denaturing (SDS-PAGE) vertical dimension. Immunoblotting was revealed with anti-RFP, -Zw10 and -Zwilch antibodies. A band in the extracts, enriched at approximately 700 kDa (indicated by a star), contains RFP-Rod, Zw10 and Zwilch (yellow rectangle).

The mutation in *RFP-rod*^{M15}changes to alanines two residues (C2011, P2012) that are almost perfectly conserved in Rod proteins between arthropods and vertebrates (Figure 2B). Uniquely among the examined mutations, *RFP-rod*^{M15} is thermosensitive in the *rod*$^{-}$ background. At 18°C, it rescues an otherwise *rod* null homozygote, generating fertile adults with normal appearance, at the expected 1:2 ratio with heterozygotes. At 29°C there are very few surviving *rod* adults (less than 5% of expected). In *rod*$^{-}$ larvae raised at 18°C and 25°C, RFP-Rod^{M15}is recruited robustly to kinetochores, but at the restrictive temperature (29°C), there is a significant reduction of RFP-Rod^{M15} kinetochore signal in *rod*$^{-}$ but not *rod*$^{+}$ cells (Figures 4A and 4B). In addition, streaming of RFP-Rod^{M15} along the spindle appeared to be reduced at 25°C in the *rod*$^{-}$ background.

To quantitate this temperature-sensitive phenotype, we compared RFP-Rod^{M15} signal normalised to Spc25-GFP after a brief (15 min) colchicine treatment, in *rod*$^{+}$ and *rod*$^{-}$ cells from larvae raised at 18°C or after a 1 h incubation at 29°C prior to dissection and treatment. As a control, cells expressing the wild-type RFP-Rod^{+} construct were similarly treated and examined (Figures 4C and 4D). RFP-Rod^{M15} kinetochore signal was profoundly reduced by the prior incubation at 29°C, in the *rod*$^{-}$ background, but not in *rod*$^{+}$. The RFP-Rod^{+} displayed no such thermolabile effect in either background.

Immunoprecipitation of RFP-Rod^{M15} from extracts of either *rod*$^{+}$ or *rod*$^{-}$ mutant animals raised at 29°C coprecipitated with Zw10 and Zwilch equally well (Figure 4E). Thus the RFP-Rod^{M15} protein is thermosensitive for its recruitment to kinetochores but not thermosensitive for RZZ assembly.

Mutations affecting streaming

Three examined Rod mutant proteins, RFP-Rod^{M7}, RFP-Rod^{M9} and RFP-Rod^{M11} were competent for at least moderate recruitment to kinetochores but had profound effects on the dynein-mediated streaming that normally carries coronal components, including RZZ, along the spindle fibres.

RFP-Rod^{M7} and *RFP-Rod*^{M9} are both capable of substantially rescuing *rod*$^{-}$ homozygotes to normal appearing but sterile adults. Consistent with this, both mutant proteins appeared well recruited to kinetochores in a *rod*$^{-}$ background (Figure 5A). As mentioned above, RFP-Rod^{M11} protein accumulated to a limited extent on kinetochores of *rod*$^{-}$ larval neuroblasts (Figures 3A, 3B, 5A). Strikingly, however, each of these three RFP-Rod variants remained largely localised at kinetochores in *rod*$^{-}$ cells, rather

Figure 4 | See Legend on next page

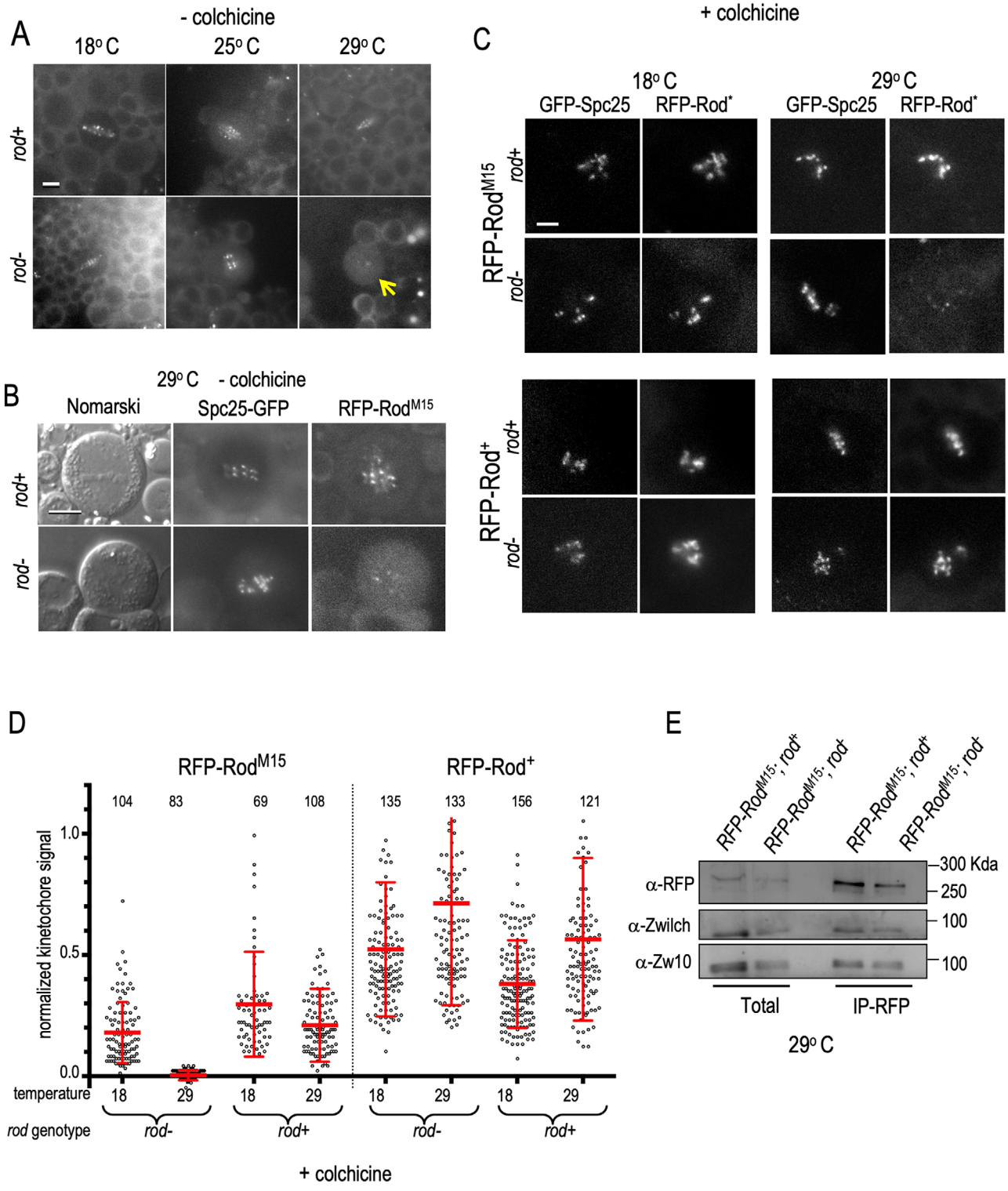

Figure 4 | *RFP-Rod^{M15}* is temperature sensitive for RZZ recruitment to kinetochores but not for its assembly
(**A**) Examples of RFP-Rod^{M15} recruitment to kinetochores at different temperatures. Live images of larval brain cells expressing RFP-Rod^{M15} at permissive temperature (18°C) intermediate temperature (25°C) and at restrictive temperature (29°C) in wild-type (top) or *rod*$^{-}$ (bottom) background. At 25°C in the absence of endogenous wild-type Rod protein, RFP-Rod^{M15} recruitment to kinetochoresis still robust but streaming along the spindle is reduced. At 29°C, recruitment to kinetochores is severely reduced (yellow arrow). Scale bar 6 microns. (**B**) RFP-Rod^{M15} kinetochore recruitment relative to Spc25-GFP (a stable component of the outer kinetochore) at 29°C. In a *rod*$^{-}$ background, RFP- Rod^{M15} recruitment is substantially reduced. Scale bar 6 microns. (**C**) Kinetochore recruitment of RFP-Rod^{M15} compared to RFP-Rod^{+} in *rod*$^{+}$ and *rod*$^{-}$ cells, at 18°C or 29°C, treated with colchicine for 15 min. In a wild-type (*rod*$^{+}$) background, RFP-Rod^{M15} is recruited robustly at both temperatures. However in a *rod*$^{-}$ background, RFP-Rod^{M15} is poorly recruited at 29°C. Spc25-GFP marks the kinetochores. (**D**) Quantitation of RFP-Rod^{M15} and RFP-Rod^{+} kinetochore signals in *rod*$^{+}$ and *rod*$^{-}$cells, normalised to that of Spc25-GFP, at 18°C or 29°C, treated with colchicine for 15 min. Each dot is the measurement of a single mitotic cell, similar to those shown in Figure 4C. Red lines correspond to the mean and SD for each set. (Note that the RFP-Rod^{+} 18°C data set also plotted in Figure 3B). Number of cells analysed per condition is indicated. (**E**) RFP-Rod^{M15} co-precipitates with Zw10 and Zwilch equally well from brain extracts of wild-type or *rod*$^{-}$ larvae raised at 29°C. Western blot of total protein extracts and anti-RFP immunoprecipitates, from third instar larval brains, revealed with anti-RFP, -Zw10 and -Zwilch antibodies.

than being distributed along the spindle, indicating reduced capacity to stream (Figure 5A and Supplemental Movie S1). To quantitate the degree of streaming, we classified cells into three categories: no streaming (RFP is found only on kinetochores), low streaming (most of the RFP signal is on kinetochores) and high streaming (RFP signal is present on kinetochores, along the spindle and at the poles). This analysis confirmed the significant reduction in streaming of these RFP-Rod^{M} proteins (Figure 5C). (Note that since streaming is a transient process, only occurring during part of metaphase, it is expected that a majority of mitotic cells will show no streaming). It also revealed a clear reduction in streaming of RFP-Rod^{M9} (see Supplemental Movie S1) and RFP-Rod^{M11} (but not RFP-Rod^{M7}) even in the *rod*$^{+}$ background, that is, in the presence of endogenous wild-type Rod protein, suggesting that these mutant proteins exert a dominant negative effect on streaming.

Because streaming is a dynein-dependent process, and since RZZ is involved in recruiting dynein to kinetochores, we asked if the lack of streaming could be correlated with loss of dynein from these kinetochores, by monitoring the GFP-tagged dynein subunit DLIC, after a brief colchicine treatment (Figure 5B). GFP-DLIC was in fact still present on kinetochores in cells expressing RFP-Rod^{M7} or RFP-Rod^{M9} in both *rod*$^{+}$ and *rod*$^{-}$ backgrounds, as well as in *rod*$^{+}$ cells expressing RFP-Rod^{M11}, but was largely absent from *RFP-Rod^{M11}*; *rod*$^{-}$ kinetochores. Thus mutant Rod proteins can interfere with streaming even though dynein is still present at kinetochores, and in the case of RFP-Rod^{M9} and RFP-Rod^{M11} even in the presence of a wild-type copy of Rod. However, RFP-Rod^{M11} appears to have a reduced capacity to recruit dynein on its own.

Discussion

We have generated mutations altering several conserved amino acids in the Rod_C domain and have found that some of these mutations profoundly impair the recruitment of RZZ to kinetochores and that others interfere with the dynein-mediated streaming of RZZ upon MT attachment.

The earliest observations of RZZ behaviour during mitosis led to the proposal that it was a major component of the fibrous corona [Basto et al., 2004; Williams et al., 1996], an expanded outer domain of unattached kinetochores that promotes microtubule capture. Features of the modelled structure of RZZ [Mosalaganti et al., 2017] display similarities to other proteins that can self-assemble into networks, such as COP1 and Clathrin, and recently several groups have reported direct cell biological and biochemical evidence for the participation of RZZ and its interacting partner Spindly in the assembly of the corona *in vivo* and filamentous structures *in vitro* ([Pereira et al., 2018; Rodriguez-Rodriguez et al., 2018; Sacristan et al., 2018], reviewed in [Suzuki and Varma, 2018]). These reports have focused particular attention on the N-terminal domain of Rod, which appears to be necessary for kinetochore expansion. The β-propeller is phosphorylated by

Figure 5 | See Legend on next page

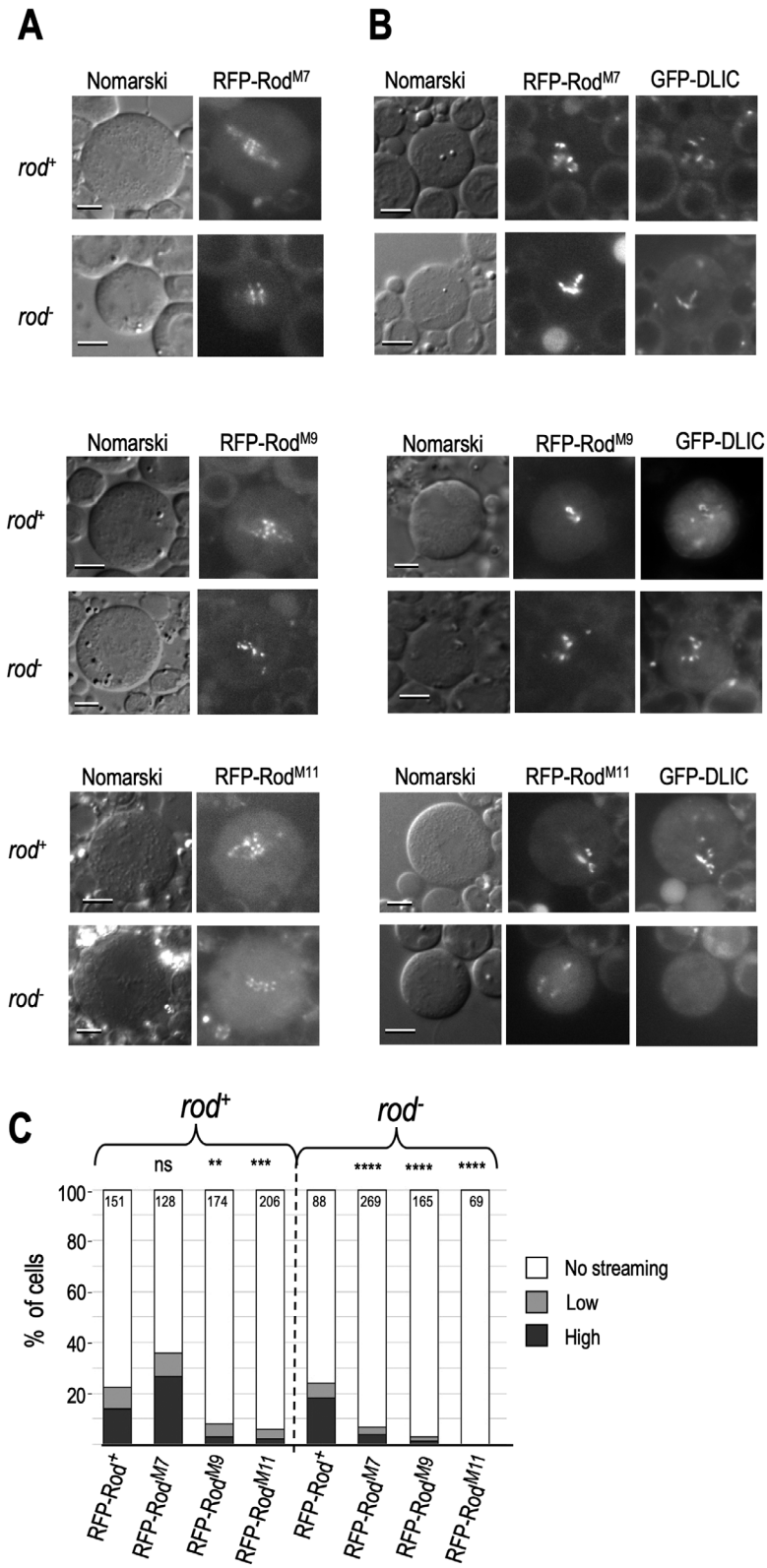

Figure 5 | *RFP-rod^{M}* mutations affecting RZZ streaming
(**A**) RFP-Rod^{M7}, RFP-Rod^{M9} and RFP-Rod^{M11} all display severe reduction in streaming. RFP-Rod^{M9} and RFP-Rod^{M11} have a semi-dominant effect on streaming, as the fraction of cells with robust streaming in a *rod*$^{+}$ background is reduced (see also Supplemental Movie S1). Live images of Nomarsky and RFP signal of larval brain cells expressing the indicated RFP-Rod^{M} variants. Scale bar 4 microns. (**B**) Despite the lack of streaming, dynein subunit GFP-DLIC is present on kinetochores in cells expressing RFP-Rod^{M7}, and RFP-Rod^{M9} in *rod*$^{-}$ background, but is absent in *RFP-Rod^{M11} rod*$^{-}$ cells. Live imaging of cells after a 15 min colchicine treatment. Scale bar 4 microns. (**C**) Quantitation of the degree of streaming of the indicated mutant RFP-Rod^{M} proteins in *rod*$^{+}$ and *rod*$^{-}$ backgrounds. Cells were classed into three degrees of streaming (high, low, none). Numbers in bars: total mitoses classed. Streaming was essentially zero for all three Rod variants in the absence of endogenous wild-type Rod (*rod*$^{-}$). Stars indicate significance of the streaming reduction compared to that of RFP-Rod^{+} : ** $p<0.002$, *** $p<0.0003$, **** $p< 0.0001$, by Fisher's exact test. NS: not significant.

Mps1 [Rodriguez-Rodriguez et al., 2018] and, along with Zwilch, [Gama et al., 2017; Pereira et al., 2018] is necessary for Spindly binding [Mosalaganti et al., 2017]. Indeed, specific mutations in Zwilch, in Spindly, and in the Rod N-terminal domain all interfere with the ability of RZZ to form expanded kinetochores *in vivo* and to oligomerise *in vitro*.

Several of mutations described here (M7, M9 and M11) severely compromise dynein-mediated streaming, similar to the previously described classical *rod^{Z3}* point mutation of the Rod_C domain [Defachelles et al., 2015a]. And like Rod^{Z3}, Rod^{M9} and Rod^{M11} both display a certain ability to dominantly interfere with streaming even in the presence of wild-type Rod, presumably a consequence of the multi-subunit nature of RZZ at kinetochores, that would incorporate copies of both mutant and wild-type Rod proteins. Moreover, Rod^{M11} seems to reduce dynein recruitment levels. Together with the temperature-sensitive Rod^{M15}, which seems to affect streaming at the semi-permissive temperature 25°C, these five mutations span about 100 amino acids of the Rod_C domain, suggesting that the integrity of this region at least is important for the proper maintenance of dynein-mediated transport of RZZ.

The interaction of dynein with RZZ is believed to be mediated by Spindly, which has been shown to bind the N-terminal domain of Rod. The fact that mutations in the Rod_C domain interfere with streaming may indicate an influence of this domain on dynein activity. Alternatively, it may be simply interfering with the ability of dynein to carry RZZ as cargo. Again, because of the head-to-tail assembly of the RZZ subunits, the Rod_C domain is presumably physically close to the regions implicated in Spindly binding.

In the RZZ structure proposed by Mosalaganti et al. [2017], the Rod_C domain would encompass a significant part of each end of the protein complex and is predicted to be in close proximity to and possibly interact with both the N-terminal β-propeller of the second Rod subunit and the Zwilch subunit. However, on the mutants where we performed co-IP tests, the altered Rod proteins co-precipitated with Zw10 and Zwilch even in the absence of wild-type Rod, and by BN-PAGE analysis, the Rod^{M5} variant assembled into a complex of similar size as wild-type RZZ. Thus the failure of mutants M5, M6 and M15 (at the restrictive temperature) to accumulate on kinetochores in *rod*$^{-}$ cells is attributable directly to the mutation and not to failure to assemble into a stable complex. Although we did not look at every mutation in this way, it seems likely that all the Rod^{M} variants capable of recruitment to kinetochores when mixed with endogenous wild-type Rod (i.e. in the *rod*$^{+}$ genetic background), necessarily retain the ability to assemble into an intact RZZ complex. We speculate that the mutant RFP-Rod^{M} proteins that were poorly expressed even in a *rod*$^{+}$ background (alleles M8, M12, M13 and M16) may in fact be unstable precisely because they failed to assemble into RZZ complexes.

It is notable that the RFP-Rod^{M} variants presented in Figures 3 and 4 displayed higher kinetochore signal in the *rod*$^{+}$ background than in *rod*$^{-}$, whereas the wild-type RFP-Rod^{+} signal was *reduced* in the *rod*$^{+}$ background. This suggests that the ability of the mutant R^{M}ZZ to accumulate on kinetochores is enhanced by association with the unlabelled endogenous Rod^{+}. In contrast, RFP-Rod^{+} would appear to be competing with the unlabelled Rod^{+} for kinetochore accumulation. These differences in behaviour support an interpretation that the lesions in the Rod^{M}

variants described here are affecting RZZ multimeric assembly into the corona.

The 16 mutations we generated were mostly designed to disrupt the charge or polarity at relatively conserved positions of the Rod_C domain. In some cases, the altered residues had been conserved since the divergence of arthropods and mammals (Figure 2B). Nevertheless, several of these mutations (M2, M3, M14, M17) functioned sufficiently well to substantially or fully rescue *rod*$^{-}$ null flies. The non-complementing mutations were nearly all within predicted α-helical sequences, which in general had conserved polarity features across phylogeny. Mutations M5 and M6, which eliminated nearly all RZZ recruitment, substituted highly conserved hydrophobic residues with glutamates. The cysteine–proline pair replaced by alanines in the mutant M15 is one of the few nearly invariant regions of the Rod_C domain that is predicted to fold into a loop between helices. The thermosensitivity of R^{M15}ZZ activity suggests that this loop may be intimately involved in the assembly of RZZ at kinetochores.

The mutations in this report argue that the Rod_C domain makes an important contribution to RZZ recruitment and functionality at the kinetochore. The *RFP-rod*^{M} alleles failing to complement the *rod* null all show partial or near-total loss of RZZ from kinetochores, but were competent to assemble with Zw10 and Zwilch. The altered amino acids of these mutants are thus prime candidates for surfaces contributing to the initial recruitment or the higher order assembly of the coronal network. In particular, the fact that colchicine treatment did not detectably increase kinetochore levels of RFP-Rod^{M5}, ^{M6} or ^{M11} (Figures 3A and 3B) suggests that they are incapable of supporting kinetochore expansion.

Materials and methods

Fly stocks

The *Drosophila* strains were raised on standard medium composition and maintained at 18, 25 or 29°C depending on the experiment. Mutations (denoted M1–M17) were generated *in vitro* in conserved amino acids in the Rod_C domain. DNA fragments encoding the Rod mutations was cloned into a previously validated pCasper4-RFP-Rod vector expressing RFP-Rod under the control of the natural endogenous *rod* promoter [Buffin et al 2005]. P-mediated fly transformation was performed by BestGene (Chino Hills, CA). The P[*RFP-Rod*^{M}] transgenes were then crossed into a stock of *rod*^{AG1}/*TM6*. *rod*^{AG1} is a null allele, bearing single nucleotide modification that changes the triplet CAA (Q) into the TAA stop codon at triplet 1004, truncating the open reading frame. In the text, '*rod*$^{+}$' refers to the heterozygous *rod*^{AG1}/*TM6* genotype. Except for Mutants 1 and 13 (for which only a single line was obtained), each mutant construct was represented by at least two independent transgenic inserts. When the transgene failed to complement *rod*$^{-}$, we tested other inserts of the same construct to exclude possible position-specific expression effects as the source of the non-complementation. Other stocks used include flies expressing RFP-Rod^{+} [Buffin et al 2005], GFP-DLIC (gift from Jordan Raff, Oxford, UK), Spc25-GFP [Schittenhelm et al., 2007] (gifts from Christian Lehner, University of Zurich, Zurich, Switzerland), GFP-Zw10 [Defachelles et al., 2015b].

Quantitation of ROD recruitment to kinetochores

For each mutant genotype, a stock containing *P{RFP-Rod*^{M}*} rod*^{AG1}*/TM6, Tb* was crossed to *P{Spc-25-GFP|y*$^{+}$*Cy; rod*^{AG1}*/TM6,Tb.* Yellow non-Tb larvae carried one copy of *RFP-Rod*^{M}, one copy of the kinetochore marker Spc25-GFP and were homozygous for *rod*^{AG1}. Sibling Tb flies were genotypically *rod*$^{+}$.

Third instar larval brains were dissected in PBS and either mounted directly under a cover slip or after incubation in colchicine (10^{-4} M) for 15 min. The brief treatment was intended to detach the microtubules from kinetochores and thus promote RZZ accumulation. Fluorescence acquisition were performed with an Olympus IX71 inverted microscope equipped for video acquisition (CellR imaging system, Xenon lamp, Hammamatsu camera), using 60× objective, NA 1.3 (see Defachelles et al. [2015a] for other details).

Live larval brains were photographed in a single optical plane. A region encompassing all the in-plane kinetochores (visible by Spc25-RFP signal) was defined, and Red and Green pixel intensities were recorded. A corresponding background signal was also acquired. The quantitation of kinetochore signal (Figures 3B and 4B) compares the recruitment of RFP-Rod^{M} in the presence (*rod*$^{+}$) and absence (*rod*$^{-}$) of endogenous Rod, in cells treated, or not, with colchicine. This 'internal' control is preferable to a comparison with a wild-type RFP-Rod recruitment, in a separately derived transgenic fly line. It also demonstrates the capacity of the transgenic construct to be incorporated into a functional RZZ complex, even when it is not functional on its own. Recruitment of a control RFP-Rod^{+} in *rod*$^{+}$ and *rod*$^{-}$ backgrounds was also measured.

Antibodies

For Western blot analysis, the following antibodies were used: rabbit anti-RFP (Abcam) and rabbit anti-Rod were diluted at 1/1000^{e}, rabbit anti-Zw10 [Williams et al.; 1992] was used at 1/2000^{e} and rabbit anti-Zwilch at 1/500^{e}. The Rabbit anti-Rod used for western blot detects many unspecific bands and was only useful for immunoblotting semi-purified samples, such as following immunoprecipitation with RFP-Trap or GFP-Trap magnetic beads. Secondary antibodies, anti-rabbit horseradish peroxidase (HRP) (Sigma Chemical Co., Saint-Quentin Fallavier, France) and anti-mouse (HRP) (Promega, Charbonnière, France) were used as described by the manufacturers.

Immunoprecipitation

Third instar larval brains were dissected in PBS and lysed in lysis buffer (ChromoTek) supplemented with 0.5% NP40 and complete anti-protease inhibitors (Roche Diagnostics) using a Dounce homogenizer. The lysates were precleared by centrifugation (2 × 20 min at 13,000 × g). For co-immunoprecipitation, 200 μg of precleared protein extract (corresponding to 120–150 brains) was incubated with 5 μL of GFP-Trap or RFP-Trap magnetic agarose beads (ChromoTek) for 1 h at 4°C on a rotating wheel. Beads were separated magnetically, and supernatant was discarded. Beads were washed twice in dilution/wash buffer (ChromoTek), and supernatant was discarded. Beads were then resuspended in 30 μL 2× SDS sample buffer and boiled 10 min at 95°C to dissociate immunocomplexes from GFP-trap or RFP-trap beads. The supernatants were then analysed by PAGE.

Blue Native PAGE electrophoresis

The experiment was performed as described by Fiala et al. [2011] and Swamy et al. [2006] and according to the user guide 'NativePAGENovexBis-Tris Gel System' from Life Technologies. Samples were prepared as follows. Third instar larval brains (120–150 brains, about 200 μg) were dissected in PBS and lysed in native PAGE sample buffer 1× (Life Technologies) supplemented with 0.5% NP40 and anti-protease inhibitors (complete from Roche Diagnostics) using a Dounce homogenizer, and the lysates were precleared by centrifugation (2 × 20 min at 13,000 × g). Samples were loaded on precast native gels (native PAGE Novex 3–12% Bis-Tris Gels, Invitrogen). Samples migrated at 150 V during 120 min at room temperature using the buffers supplied. The lane of the native gel containing the sample of interest was excised and denatured in NuPAGE LDS Sample Buffer (1×) and NuPAGE Sample Reducing (1×) (Life Technologies). The strip was loaded onto a second dimension SDS-PAGE gel (6%), and electrophoresis was performed by standard protocols. The Coomassie staining of the native gels was performed using the PAGE Blue Staining Solution (Thermo Fisher Scientific).

Author contribution

Concept and design of experiments: AM and RK. Experimental work: AM. Data analysis, interpretation, writing: AM and RK.

Funding

This work in the RK's laboratory was supported by the Centre National de la Recherche Scientifique (CNRS), Agence Nationale de la Recherche #ANR-08-BLAN-0006; La Ligue National Contre le Cancer Equipe Labellisée program 2012 and La Fondation ARC pour la Recherche sur le Cancer. This study contributes to the LabEx "Who Am I?" #ANR-11-LABX-0071 and the Université de Paris IdEx #ANR-18-IDEX-0001 funded by the French Government through its 'Investments for the Future' programme.

Acknowledgements

We thank V. Doye and C. Jackson for suggestions and stimulating discussions.

Conflict of interest

The authors have declared no conflict of interest.

References

Basto, R., Scaerou, F., Mische, S., Wojcik, E., Lefebvre, C., Gomes, R., Hays, T. and Karess, R. (2004) In vivo dynamics of the rough deal checkpoint protein during *Drosophila* mitosis. Curr. Biol **14**, 56–61

Buffin, E., Lefebvre, C., Huang, J., Gagou, M.E. and Karess, R.E. (2005) Recruitment of Mad2 to the kinetochore requires the Rod/Zw10 complex. Curr. Biol. **15**, 856–61

Caldas, G.V., Lynch, T.R., Anderson, R., Afreen, S., Varma, D. and DeLuca, J.G. (2015) The RZZ complex requires the N-terminus of KNL1 to mediate optimal Mad1 kinetochore localization in human cells. Open Biol. 5, 150160

Chan, Y.W., Fava, L.L., Uldschmid, A., Schmitz, M.H., Gerlich, D.W., Nigg, E.A. and Santamaria, A. (2009) Mitotic control of kinetochore-associated dynein and spindle orientation by human Spindly. J. Cell Biol. **185**, 859–74

Cheerambathur, D.K., Gassmann, R., Cook, B., Oegema, K. and Desai, A. (2013) Crosstalk between microtubule attachment complexes ensures accurate chromosome segregation. Science **342**, 1239–42

Civril, F., Wehenkel, A., Giorgi, F.M., Santaguida, S., Di Fonzo, A., Grigorean, G., Ciccarelli, F.D. and Musacchio, A. (2010) Structural analysis of the RZZ complex reveals common ancestry with multisubunit vesicle tethering machinery. Structure **18**, 616–26

Defachelles, L., Hainline, S.G., Menant, A., Lee, L.A. and Karess, R.E. (2015a). A maternal effect rough deal mutation suggests that multiple pathways regulate *Drosophila* RZZ kinetochore recruitment. J. Cell Sci. **128**, 1204–16

Defachelles, L., Raich, N., Terracol, R., Baudin, X., Williams, B., Goldberg, M. and Karess, R.E. (2015b). RZZ and Mad1 dynamics in *Drosophila* mitosis. Chromosome Res. **23**, 333–342

Fiala, G.J., Schamel, W.W. and Blumenthal, B. (2011) Blue Native polyacrylamide gel electrophoresis (BN-PAGE) for analysis of multiprotein complexes from cellular lysates. J. Vis. Exp. **2011**, 2164

Gama, J.B., Pereira, C., Simoes, P.A., Celestino, R., Reis, R.M., Barbosa, D.J., Pires, H.R., Carvalho, C., Amorim, J., Carvalho, A.X. et al. (2017) Molecular mechanism of dynein recruitment to kinetochores by the Rod-Zw10-Zwilch complex and Spindly. J. Cell Biol. **216**, 943–960

Gassmann, R., Essex, A., Hu, J.S., Maddox, P.S., Motegi, F., Sugimoto, A., O'Rourke, S.M., Bowerman, B., McLeod, I., Yates, J.R., 3rd et al. (2008) A new mechanism controlling kinetochore-microtubule interactions revealed by comparison of two dynein-targeting components: SPDL-1 and the Rod/Zwilch/Zw10 complex. Genes Dev. **22**, 2385–99

Gassmann, R., Holland, A.J., Varma, D., Wan, X., Civril, F., Cleveland, D.W., Oegema, K., Salmon, E.D. and Desai, A. (2010) Removal of Spindly from microtubule-attached kinetochores controls spindle checkpoint silencing in human cells. Genes Dev. **24**, 957–71

Griffis, E.R., Stuurman, N. and Vale, R.D. (2007) Spindly, a novel protein essential for silencing the spindle assembly checkpoint, recruits dynein to the kinetochore. J. Cell Biol. **177**, 1005–15

Karess, R. (2005) Rod-Zw10-Zwilch: a key player in the spindle checkpoint. Trends Cell Biol. **15**, 386–92

Kops, G.J., Kim, Y., Weaver, B.A., Mao, Y., McLeod, I., Yates, J.R., 3rd, Tagaya, M. and Cleveland, D.W. (2005) ZW10 links mitotic checkpoint signaling to the structural kinetochore. J. Cell Biol **169**, 49–60

Marchler-Bauer, A., Bo, Y., Han, L., He, J., Lanczycki, C.J., Lu, S., Chitsaz, F., Derbyshire, M.K., Geer, R.C., Gonzales, N.R. et al. (2017) CDD/SPARCLE: functional classification of proteins via subfamily domain architectures. Nucleic Acids Res. **45**, D200–D203

Mosalaganti, S., Keller, J., Altenfeld, A., Winzker, M., Rombaut, P., Saur, M., Petrovic, A., Wehenkel, A., Wohlgemuth, S., Muller, F. et al. (2017) Structure of the RZZ complex and molecular basis of its interaction with Spindly. J. Cell Biol. **216**, 961–981

Musacchio, A. (2015) The molecular biology of spindle assembly checkpoint signaling dynamics. Curr. Biol. **25**, R1002-18

Pereira, C., Reis, R.M., Gama, J.B., Celestino, R., Cheerambathur, D.K., Carvalho, A.X. and Gassmann, R. (2018) Self-assembly of the RZZ complex into filaments drives kinetochore expansion in the absence of microtubule attachment. Curr. Biol. **28**, 3408–3421.e8

Rodriguez-Rodriguez, J.A., Lewis, C., McKinley, K.L., Sikirzhytski, V., Corona, J., Maciejowski, J., Khodjakov, A., Cheeseman, I.M. and Jallepalli, P.V. (2018) Distinct roles of RZZ and Bub1-KNL1 in mitotic checkpoint signaling and kinetochore expansion. Curr. Biol. **28**, 3422–3429 e5

Sacristan, C., Ahmad, M.U.D., Keller, J., Fermie, J., Groenewold, V., Tromer, E., Fish, A., Melero, R., Carazo, J.M., Klumperman, J. et al. (2018) Dynamic kinetochore size regulation promotes microtubule capture and chromosome biorientation in mitosis. Nat. Cell Biol. **20**, 800–810

Scaerou, F., Starr, D.A., Piano, F., Papoulas, O., Karess, R.E. and Goldberg, M.L. (2001) The ZW10 and Rough Deal checkpoint proteins function together in a large, evolutionarily conserved complex targeted to the kinetochore. J. Cell Sci. **114**, 3103–3114

Schittenhelm, R.B., Heeger, S., Althoff, F., Walter, A., Heidmann, S., Mechtler, K. and Lehner, C.F. (2007) Spatial organization of a ubiquitous eukaryotic kinetochore protein network in Drosophila chromosomes. Chromosoma **116**, 385–402

Silio, V., McAinsh, A.D. and Millar, J.B. (2015) KNL1-Bubs and RZZ provide two separable pathways for checkpoint activation at human kinetochores. Dev. Cell **35**, 600–613

Starr, D.A., Williams, B.C., Hays, T.S. and Goldberg, M.L. (1998) ZW10 helps recruit dynactin and dynein to the kinetochore. J. Cell Biol. **142**, 763–774

Suzuki, A. and Varma, D. (2018) Cell division: the unattached kinetochore wears an expansive RZZ coat. Curr. Biol. **28**, R1250–R1252

Swamy, M., Kulathu, Y., Ernst, S., Reth, M. and Schamel, W.W. (2006) Two dimensional Blue Native-/SDS-PAGE analysis of SLP family adaptor protein complexes. Immunol. Lett. **104**, 131–137

Williams, B.C., Gatti, M. and Goldberg, M.L. (1996) Bipolar spindle attachments affect redistributions of ZW10, a *Drosophila* centromere/kinetochore component required for accurate chromosome segregation. J. Cell Biol. **134**, 1127–40

Williams, B.C. and Goldberg, M.L. (1994) Determinants of *Drosophila* zw10 protein localization and function. J. Cell Sci. **107** (Pt 4), 785–98

Williams, B.C., Karr, T.L., Montgomery, J.M. and Goldberg, M.L. (1992) The *Drosophila* l(1)zw10 gene product, required for accurate mitotic chromosome segregation, is redistributed at anaphase onset. J. Cell Biol. **118**, 759–73

Williams, B.C., Li, Z., Liu, S., Williams, E.V., Leung, G., Yen, T.J. and Goldberg, M.L. (2003) Zwilch, a new component of the ZW10/ROD complex required for kinetochore functions. Mol. Biol. Cell **14**, 1379–91

Zhang, G., Lischetti, T., Hayward, D.G. and Nilsson, J. (2015) Distinct domains in Bub1 localize RZZ and BubR1 to kinetochores to regulate the checkpoint. Nat. Commun. **6**, 7162

Received: 12 December 2019; Revised: 29 May 2020; Accepted: 3 June 2020; Accepted article online: 30 June 2020